AGU PUBLICATIONS

Geophysical Research Letters

RESEARCH LETTER
10.1002/2015GL066198

Key Points:
- The positive gravity signature of craters is due to initial porosity compaction
- Porosity is responsible for the observed scatter in the Bouguer anomalies
- Mantle uplift dominates the gravity for craters larger than ~215 km in diameter

Supporting Information:
- Texts S1–S4 and Tables S1–S3
- Figure S1
- Figure S2
- Figure S3
- Figure S4

Correspondence to:
C. Milbury,
cmilbury@purdue.edu

Citation:
Milbury, C., B. C. Johnson, H. J. Melosh, G. S. Collins, D. M. Blair, J. M. Soderblom, F. Nimmo, C. J. Bierson, R. J. Phillips, and M. T. Zuber (2015), Preimpact porosity controls the gravity signature of lunar craters, *Geophys. Res. Lett.*, *42*, 9711–9716, doi:10.1002/2015GL066198.

Received 14 SEP 2015
Accepted 1 NOV 2015
Accepted article online 4 NOV 2015
Published online 19 NOV 2015

Preimpact porosity controls the gravity signature of lunar craters

C. Milbury[1], B. C. Johnson[2,3], H. J. Melosh[1], G. S. Collins[4], D. M. Blair[5], J. M. Soderblom[2], F. Nimmo[6], C. J. Bierson[6], R. J. Phillips[7], and M. T. Zuber[2]

[1]Department of Earth, Atmospheric, and Planetary Sciences, Purdue University, West Lafayette, Indiana, USA, [2]Department of Earth, Atmospheric and Planetary Sciences, Massachusetts Institute of Technology, Cambridge, Massachusetts, USA, [3]Now at Department of Earth, Environmental and Planetary Science, Brown University, Providence, Rhode Island, USA, [4]Earth Science and Engineering Department, Imperial College London, London, UK, [5]Haystack Observatory, Massachusetts Institute of Technology, Westford, Massachusetts, USA, [6]Department of Earth and Planetary Sciences, University of California, Santa Cruz, California, USA, [7]Planetary Science Directorate, Southwest Research Institute, Boulder, Colorado, USA

Abstract We model the formation of lunar complex craters and investigate the effect of preimpact porosity on their gravity signatures. We find that while preimpact target porosities less than ~7% produce negative residual Bouguer anomalies (BAs), porosities greater than ~7% produce positive anomalies whose magnitude is greater for impacted surfaces with higher initial porosity. Negative anomalies result from pore space creation due to fracturing and dilatant bulking, and positive anomalies result from destruction of pore space due to shock wave compression. The central BA of craters larger than ~215 km in diameter, however, are invariably positive because of an underlying central mantle uplift. We conclude that the striking differences between the gravity signatures of craters on the Earth and Moon are the result of the higher average porosity and variable porosity of the lunar crust.

1. Introduction

Complex craters on the Moon are associated with both positive and negative Bouguer gravity anomalies [*Soderblom et al.*, 2015], unlike their terrestrial counterparts, which invariably exhibit negative Bouguer gravity anomalies [*Pilkington and Grieve*, 1992]. Furthermore, craters located in the South Pole-Aitken (SP-A) basin and maria tend to have more negative signatures than those located in the highlands [*Phillips et al.*, 2015]. Data from NASA's Gravity Recovery and Interior Laboratory (GRAIL) mission [*Zuber et al.*, 2013] show that the porosity of the Moon's crust varies substantially both laterally [*Wieczorek et al.*, 2013] and vertically [*Besserer et al.*, 2014].

Early in a hypervelocity impact, a hemispherical shock wave passes through the target and compresses material adjacent to the impact site. Close to the point of impact, the shock wave crushes out any preexisting pore space [*Wünnemann et al.*, 2006; *Collins et al.*, 2011]. Because the shock wave decays as it expands, preimpact pore space farther from the point of impact remains intact. After passage of the shock wave and the rarefaction that follows it, the excavation creates a bowl-shaped transient crater that ejects low-density porous material in the process. The transient crater then collapses under gravitational forces. The associated deformation of displaced material creates pore space through dilatant expansion [*Reynolds*, 1885], resulting in a lower density material that exhibits a negative Bouguer anomaly (BA), as is observed for nearly all terrestrial craters [*Pilkington and Grieve*, 1992; *Collins*, 2014]. The maximum negative gravity anomaly of terrestrial craters increases in magnitude with crater diameter (D) [*Pilkington and Grieve*, 1992]. Although lunar craters exhibit a similar trend, their gravity anomalies can be positive or negative, exhibiting a surprisingly large scatter of ±25 mGal about their mean [*Soderblom et al.*, 2015]. For craters larger than a certain D, mantle uplift produces large positive gravity anomalies as observed in lunar mascon basins [*Melosh et al.*, 2013; *Freed et al.*, 2014]. The dominant factor that controls the gravity signature of lunar craters depends on the competing effects of the compaction of preexisting pore space and the creation of new pore space during deformation of geologic materials (dilatancy) for relatively smaller complex craters, with the additional effect of mantle uplift for relatively larger craters that sample greater depth. *Collins* [2014] implemented a hydrocode model for dilatancy and used it to successfully reproduce the observed gravity anomalies of terrestrial craters but did not examine the role of preimpact target porosity, which is generally

Table 1. Impactor and Final Craters Diameters for the Simulations Plotted in Figures 1 and 2

$D_{impactor}$ (km)	D_{crater} (km)		
Porosity (%)	0	6.8	13.6
3	54	46	46
6	96	90	90
8	132	116	118
10	160	148	144
12	182	174	172
14	210	204	202
18	284	266	256
24	390	350	320
30	450	420	406

believed to be small on Earth. However, the lunar crust is highly fractured and porous, plausibly resembling that of the Hadean Earth. For the first time, we have modeled preimpact porosity and dilatancy together to determine their relative effects on the geophysical structure, and thereby gravity signature, of lunar impact craters.

2. Methods

We simulate crater formation using the iSALE shock physics code [*Collins et al*., 2004; *Wünnemann et al*., 2006], which is an extension of the SALE hydrocode [*Amsden et al*., 1980]. To simulate hypervelocity impact processes in solid materials, SALE was modified to include an elastic-plastic constitutive model, fragmentation models, various equations of state (EoS), and multiple materials [*Melosh et al*., 1992; *Ivanov et al*., 1997]. More recent improvements include a modified strength model [*Collins et al*., 2004], a porosity compaction model [*Wünnemann et al*., 2006; *Collins et al*., 2011], and the creation of porosity by dilatancy [*Collins*, 2014]. Due to computational limitations, all of the computations here assume axial symmetry, so the impacts are necessarily vertical. Nine different impactor sizes were used, ranging in size from 3 to 30 km in diameter. The upper few kilometers of the crust of the Moon has an average porosity of ~12% [*Wieczorek et al*., 2013]. This porosity decreases with depth, resulting in an average porosity of ~6% over the entire vertical extent of the crust [*Besserer et al*., 2014]. We investigated three different preimpact porosities: 0, 6.8, and 13.6%. We used a crustal thickness of 35 km, comparable to the Moon's average value [*Wieczorek et al*., 2013]. (See the supporting information for a full description of the modeling setup and parameters).

To model impact-induced density changes owing to the destruction and creation of pore space, we employed iSALE's porous compaction [*Wünnemann et al*., 2006; *Collins et al*., 2011] and dilatancy [*Collins*, 2014] algorithms in tandem. Table 1 lists the impactor diameter and rim-to-rim final crater diameter (defined as twice the radius of the highest output topography) for each porosity value that we investigated. The small number of equations of state (EoS) that can accurately represent the behavior of geologic material shocked to high temperatures forces us to make approximations using the best available EoS. Thus, we used equation of state tables produced using the Analytical Equation of State [*Thompson and Lauson*, 1972] package with input parameters for granite [*Pierazzo et al*., 1997] to approximate the lunar crust, and dunite [*Benz et al*., 1989] for the lunar mantle and impactor.

For each of the simulations listed in Table 1, the following model parameters were used: a typical impact velocity for the Moon of 15 km/s [*Yue et al*., 2013], a surface gravity of 1.6249 m/s^2, a surface temperature of 300 K, and a thermal gradient of 5 K/km (which is consistent with current estimates). We use a conductive thermal profile for depths of up to 200 km and a convective thermal profile given by an adiabatic thermal gradient of about 0.5 K/km for depths in excess of 200 km. The left/right velocity boundary conditions were free slip, and the top/bottom were outflow/no slip, respectively. We used strength parameters of gabbroic anorthosite to describe the crust and those of dunite to describe the mantle and impactor [*Potter et al*., 2013]. We used 35 km as the crustal thickness, which is consistent with average values [*Wieczorek et al*., 2013], because the aim of this investigation was to match global observations of the gravity signature of craters. See the supporting information for a complete list of the material and mesh parameters used in the simulations.

Acoustic fluidization (AF) represents the behavior of fractured rock as a viscous fluid [*Melosh*, 1989] and is triggered by intense, short-wavelength vibrations within the target. It was proposed as a mechanism to temporarily weaken rock, which is required to describe the collapse phase of crater formation. We used the block model [*Melosh and Ivanov*, 1999; *Ivanov and Artemieva*, 2002; *Wünnemann and Ivanov*, 2003] of AF for this analysis. The AF input parameters were selected on the basis that the final simulated crater shape produced by a 6 km impactor provided the best fit to observed crater morphology [*Kalynn et al*., 2013] and is described fully in Text S1 of the supporting information. The parameters for the porous versus nonporous

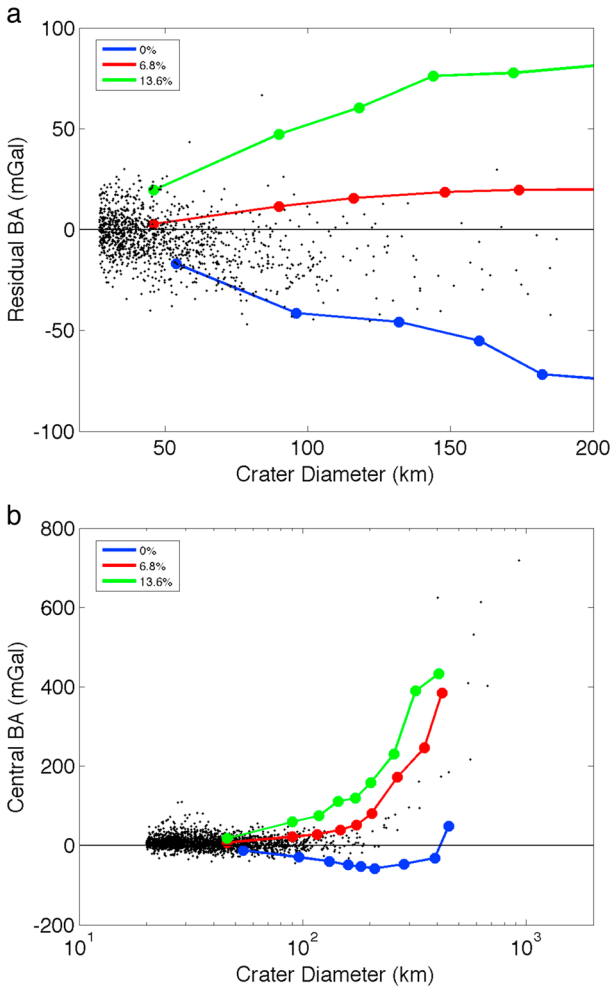

Figure 1. Bouguer anomalies for observed and simulated craters on the Moon. (a) Plot of the residual Bouguer anomaly (BA) as a function of *D* for the simulations performed here. The blue dots represent 0% initial porosity, the red dots are for 6.8% porosity models, the green dots are the 13.6% porosity models, and the black stars represent the data from *Soderblom et al.* [2015]. (b) Plot of the central BA, where the symbols are the same for Figure 1a.

targets are different because the shock wave is more strongly attenuated in targets with substantial porosity [*Milbury et al.*, 2014].

The dilatancy model parameters used in this analysis were based on calibration of the dilatancy model with data from terrestrial craters [*Collins*, 2014]. In the terrestrial study, a range of dilatancy coefficients were tested for rock masses with a low, average, and high quality Geological Strength Index (GSI). A value of 0.045, corresponding to low-quality GSI, was found to fit the observations best for simple craters, was used in this study, and is not expected to change significantly for complex craters. The compaction model parameters used in this study are described in *Wünnemann et al.* [2006] and are given in the supporting information.

We investigated the effect of impact velocity and crustal thickness on the BA. For each of the simulations we used an 8 km impactor and an initial target porosity of 6.8%. The BA for impact velocities of 6, 9, and 12 km/s are compared with the nominal case of 15 km/s (see Figure S2). As the impact velocity decreases, the size of the crater decreases because there is less energy to open the crater. The amount of impactor that is vaporized also decreases, and some of the impactor survives [*Yue et al.*, 2013], so there is an apparent BA from the impactor (dashed lines on Figure S2). If this is subtracted from the BA, then the 6 and 9 km/s simulations have the greatest BA by ~5–10 mGal at the very center, which is somewhat surprising. However, this is due to the fact that higher impactor velocities generate more heat and therefore heat the material to higher temperature, which decreases the crustal density and thus decreases the BA. We calculate the change in BA due to subsequent thermal contraction and find an increase of less than 10 mGal (see the supporting information), which makes the BA for the 6 and 9 km/s runs more similar to the nominal 15 km/s run.

We also investigated the effect of varying crustal thickness on our results (see Figure S3), which is more important for large impactors because they penetrate through more crust than small impactors. Decreasing the crustal thickness has the effect of increasing the BA in the center of the crater because of enhanced mantle uplift; i.e., areas of the Moon with thinner crust will have BA associated with mantle uplift at smaller *D* than areas with thicker crust. This is part of the reason that there is a range of crater diameter where the central BA transitions from (essentially) zero to positive values.

The calculation of the gravity anomalies associated with the simulated craters is the same as that used in the analysis of the lunar mascon basins [*Melosh et al.*, 2013; *Freed et al.*, 2014]. We calculate the gravity anomalies at an altitude that was approximately 1 km above the rim of the final crater; however, the gravity anomaly is not sensitive to small changes in altitude.

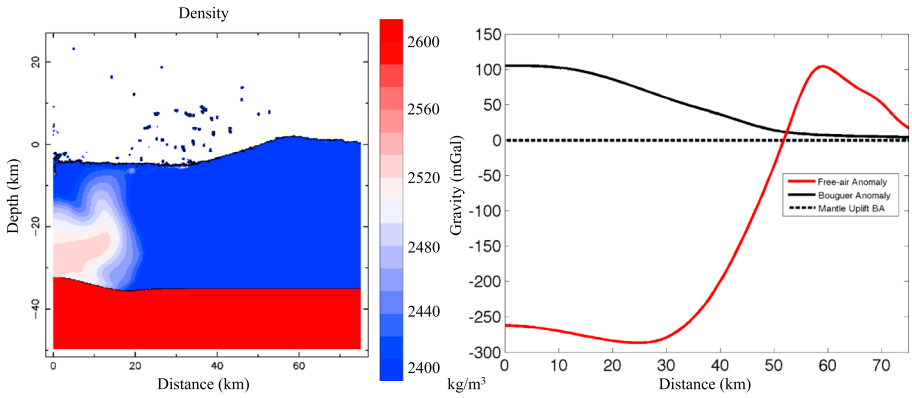

Figure 2. Density for a modeled lunar crater exhibiting a positive Bouguer anomaly. (left) The resulting density structure for a simulated crater with an initial target porosity of 13.6% and an 8 km diameter impactor. (right) The Bouguer anomaly (black), BA due to mantle uplift alone (black dashed), and the free air anomaly (red) versus distance from the center of the crater.

One factor that we are unable to investigate in our 2-D simulations is the effect of impact angle. Previous studies [*Pierazzo and Melosh*, 2000; *Elbeshausen et al*., 2013] have shown that unless the impact angle is greater than about 75° with respect to the normal, crater shape is nearly indistinguishable from that formed by a vertical impact, but those studies did not include porosity. It is thus possible that some of the observed scatter in BA is due to impact angle, a factor that will require future investigation.

3. Results

For each run, we calculated the gravity anomaly associated with the simulated craters [*Melosh et al*., 2013; *Freed et al*., 2014], and the residual BA, the metric derived to investigate lunar impacts using GRAIL gravity data. The residual BA is the area-weighted mean BA calculated interior to the crater rim less the mean BA within a background annulus of width and inner radius equal to the crater radius [*Soderblom et al*., 2015]. The results of the simulations listed in Table 1 are shown in Figure 1a (colored dots) for comparison with the observations [*Soderblom et al*., 2015] (black dots). For a given crater size, the magnitude of the residual BA increases with increasing porosity. For the modeled range of preimpact porosity, our model results bound the observed BAs of complex craters [*Soderblom et al*., 2015].

Thus, the scatter in the observed residual BA can be explained by variations in preimpact crustal porosity. This is supported by the apparent correlation of background porosity with the magnitude of the residual BA [*Soderblom et al*., 2015]. A relatively high initial porosity results in a positive BA because the shock wave generated by the impact crushes out pore space most effectively near the center of the crater, leaving a higher bulk density than the preimpact bulk density (see Figure 2). Additionally, when pore space is crushed out, it also heats up the material, which decreases the creation of pore space by dilatancy as the material begins to melt [*Collins*, 2014]. Conversely, relatively lower initial preimpact porosities lead to negative BAs because dilatancy is more effective than pore space compaction. We find that thermal contraction subsequent to impact-induced heating increases the calculated BA by a minimal amount (typically $<$10 mGal; see supporting information), and so we do not make corrections to account for this effect. Porosity is not the sole source of the observed scatter in the BA, and there are other influences such as impact angle and velocity, crustal thickness variations, heterogeneities, and other factors that will also contribute to variations in crater gravity (see supporting information).

Figure 1a shows that the negative trend of the residual BA with increasing *D* is only present for simulations that have a low initial porosity. The observation that relatively small craters tend to have a more positive residual anomaly than larger craters could be attributed to an increase in the density of fracturing with *D* [*Soderblom et al*., 2015]. Another contributing factor may be the vertical porosity gradients that have been detected in the lunar crust [*Besserer et al*., 2014]; i.e., if porosity generally decreases with depth, smaller impacts will affect portions of the crust with higher porosity than larger impacts do and, therefore, based

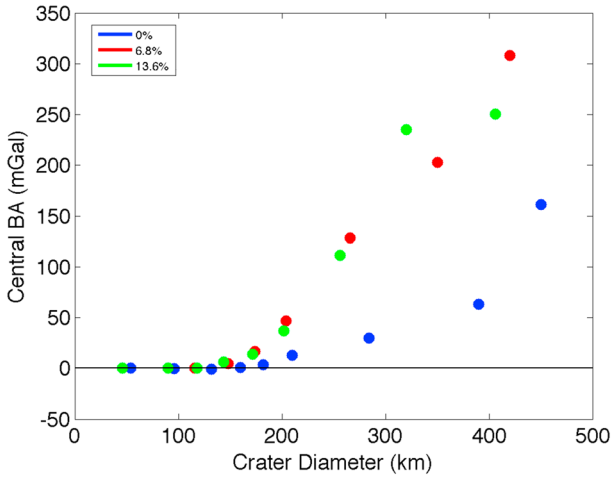

Figure 3. Central Bouguer anomaly transition from mantle uplift. Central BA due solely to mantle uplift for small crater D, showing the transition for zero to positive values that occurs for $D \sim 140$–215 km. The blue, red, and green dots represent models with 0%, 6.8%, and 13.6% initial porosity, respectively.

on our models, will result in a more positive residual BA. This is consistent with the observation that craters within SP-A, which has a thinner low-density (porous) layer than the rest of the farside [*Besserer et al.*, 2014], have more negative residual BA signatures [*Phillips et al.*, 2015].

Our results indicate that the striking difference between the gravity anomalies of lunar and terrestrial impact craters is due to initial porosity of the lunar crust. The negative gravity anomalies commonly associated with terrestrial craters [*Pilkington and Grieve*, 1992] are a result of the Earth's porosity structure. The Earth's crust is typically less than a few percent porous [*Hyndman and Klemperer*, 1989; *Aquilina et al.*, 2004], whereas the lunar crust is 6% porous on average [*Besserer et al.*, 2014]. Additionally, the depth at which pore space closure occurs on Earth [*Manning and Ingebritsen*, 1999] is much shallower than for the Moon [*Besserer et al.*, 2014]. Lastly, the Earth and Moon have very different geologic and evolutionary histories, which would also influence crater gravity signatures.

3.1. Transition From Porosity-Dominated Regime to Mantle Uplift-Dominated Regime

The central BA, which is different from the residual BA, is sensitive to the excess mass beneath the central region of the crater caused by mantle uplift during transient crater collapse. The central BA is the area-weighted mean BA from the center to 0.2 rim radii less the area-weighted mean BA within an annulus that extends from 0.5 to 1.0 rim radius. The central BA values of highland craters exhibits a break in the slope for $D > 218 \pm 17$ km, which is interpreted as the onset of mantle uplift [*Soderblom et al.*, 2015].

Our model results exhibit a similar transition (see Figure 1b) and allow us to directly determine the diameter above which mantle uplift begins to dominate the gravity signature. To isolate the signature of the mantle uplift and ignore other factors affecting material density (pressure, temperature, and porosity), all crustal material was given a density of 2550 kg/m^3, and all mantle material was given a density of 3220 kg/m^3. This ensures that the density contrast, and therefore the gravity anomaly, arises solely from the crust-mantle interface and not from density variations within each unit. Figure 3 shows that the contribution from mantle uplift to the BA is zero until $D \sim 140$ km and that it does not exceed the ±25 mGal scatter until $D \sim 215$ km. Our results show that preimpact porosity is the dominant control on the BA until $D \sim 140$ km and that mantle uplift dominates the BA for $D > 215$ km.

Figure 3 shows that mantle uplift cannot explain the scatter of BAs for relatively smaller craters. The source of that variation is likely spatial heterogeneity of preimpact porosity in the crust. The diameter at which the porosity-dominated regime changes to mantle uplift-dominated regime coincides with the morphological transition from central peak craters to peak ring basins, which may be coincidental on the Moon. For example, the Chicxulub impact basin on Earth is a peak ring basin, but seismic methods have revealed only minor (<2 km) deflection of the crust-mantle boundary [*Christeson et al.*, 2009]. Our results indicate that impacts into a target that is highly porous will destroy porosity and produce a positive BA, while impacts into a less porous crust will create porosity and produce a negative BA.

4. Summary and Conclusions

Our modeling shows that over time, impacts are capable of producing global changes in crustal porosity, both increases and decreases. Understanding the creation and destruction of porosity by impacts is a crucial first step toward understanding how the porosity of the crust evolves with depth and time. Because changes

in porosity also lead to changes in permeability and thermal conductivity of planetary crusts, impact-induced changes to porosity have important implications for the thermal, magmatic, and, where applicable, hydrologic evolution of ancient planetary crusts throughout the solar system.

Acknowledgments
We thank all those involved with the development and operations of the GRAIL spacecraft and the collection and reduction of the GRAIL data. This work was funded in part by the GRAIL mission, which is supported by the NASA Discovery Program and is performed under contract to the Massachusetts Institute of Technology and the Jet Propulsion Laboratory, California Institute of Technology. We thank Boris Ivanov for an insightful and helpful review that improved the quality of this paper. We gratefully acknowledge the developers of iSALE, including Kai Wünnemann, Dirk Elbeshausen, Boris Ivanov, and Tom Davison. G.S.C. acknowledges funding from Science and Technologies Research Council grant ST/J001260/1.

References

Amsden, A. A., H. M. Ruppel, and C. W. Hirt (1980), SALE: A simplified ALE computer program for fluid flow at all speeds, Los Alamos Nat. Lab. Rep., LA-8095: 101 p, LANL.

Aquilina, L., J. Dreuzy, O. Bour, and P. Davy (2004), Porosity and fluid velocities in the upper continental crust (2 to 4 km) inferred from injection tests at the Soultz-sous-Forêts geothermal site, *Geochim. Cosmochim. Acta*, *68*, 2405–2415.

Benz, W., A. G. W. Cameron, and H. J. Melosh (1989), The origin of the Moon and the single-impact hypothesis III, *Icarus*, *81*, 113–131.

Besserer, J., F. Nimmo, M. A. Wieczorek, R. C. Weber, W. S. Kiefer, P. J. McGovern, J. C. Andrews-Hanna, D. E. Smith, and M. T. Zuber (2014), GRAIL gravity constraints on the vertical and lateral density structure of the lunar crust, *Geophys. Res. Lett.*, *41*, 5771–5777, doi:10.1002/2014GL060240.

Collins, G. S. (2014), Numerical simulations of impact crater formation with dilatancy, *J. Geophys. Res. Planets*, *119*, 2600–2619, doi:10.1002/2014JE004708.

Collins, G. S., H. J. Melosh, and B. A. Ivanov (2004), Modeling damage and deformation in impact simulations, *Meteorit. Planet. Sci.*, *39*, 217–231.

Collins, G. S., H. J. Melosh, and K. Wünnemann (2011), Improvements to the epsilon-alpha porous compaction model for simulating impacts into high-porosity solar system objects, *Int. J. Impact Eng.*, *38*, 434–439.

Christeson, G. L., G. S. Collins, J. V. Morgan, S. P. S. Gulick, P. J. Barton, and M. R. Warner (2009), Mantle deformation beneath the Chicxulub impact crater, *Earth Planet. Sci. Lett.*, doi:10.1016/10.1016/j.epsl.2009.04.033.

Elbeshausen, D., K. Wünnemann, and G. S. Collins (2013), The transition from circular to elliptical craters, *J. Geophys. Res. Planets*, *118*, 2295–2309.

Freed, A. M., B. C. Johnson, D. M. Blair, H. J. Melosh, G. A. Neumann, R. J. Phillips, S. C. Solomon, M. A. Wieczorek, and M. T. Zuber (2014), The formation of lunar mascon basins from impact to contemporary form, *J. Geophys. Res. Planets*, *119*, 2378–2397, doi:10.1002/2014JE004657.

Hyndman, R. D., and S. L. Klemperer (1989), Lower-crustal porosity from electrical measurements and inferences about composition from seismic velocities, *Geophys. Res. Lett.*, *16*, 255–258, doi:10.1029/GL016i003p00255.

Ivanov, B. A., and N. A. Artemieva (2002), Numerical modeling of the formation of large impact craters, in catastrophic events and mass extinctions: Impact and beyond, *Geol. Soc. Am. Spec. Pap.*, *356*, 619–630, doi:10.1130/0-8137-2356-6.619.

Ivanov, B. A., D. Deniem, and G. Neukum (1997), Implementation of dynamic strength models into 2D hydrocodes: Applications for atmospheric breakup and impact cratering, *Int. J. Impact Eng.*, *20*(1–5), 411–430.

Kalynn, J., C. L. Johnson, G. R. Osinski, and O. Barnouin (2013), Topographic characterization of lunar complex craters, *Geophys. Res. Lett.*, *40*, 38–42, doi:10.1029/2012GL053608.

Manning, C. E., and S. E. Ingebritsen (1999), Permeability of the continental crust: Implications of geothermal data and metamorphic systems, *Rev. Geophys.*, *37*(1), 127–150, doi:10.1029/1998RG900002.

Melosh, H. J. (1989), *Impact Cratering: A Geologic Process*, Oxford Univ. Press, New York.

Melosh, H. J., and B. A. Ivanov (1999), Impact crater collapse, *Ann. Rev. Earth Planet. Sci.*, *27*, 385–415.

Melosh, H. J., E. V. Ryan, and E. Asphaug (1992), Dynamic fragmentation in impacts: Hydrocode simulation of laboratory impacts, *J. Geophys. Res.*, *97*(E9), 14,735–14,759, doi:10.1029/92JE01632.

Melosh, H. J., et al. (2013), The origin of lunar mascon basins, *Science*, *340*, 1552–1555, doi:10.1126/science.1235768.

Milbury, C., B. C. Johnson, H. J. Melosh, D. M. Blair, and G. S. Collins (2014), The effects of porosity on lunar crater formation and the transition from complex crater to peak ring basin morphology, LPSC Conference, XLV: Abstract 2270.

Phillips, R. J., C. J. Thomason, J. W. Head, J. M. Soderblom, F. Nimmo, J. Besserer, H. J. Melosh, C. Milbury, W. S. Kiefer, and M. T. Zuber (2015), Crater Bouguer anomalies probe South Pole-Aitken (SPA) basin structure, LPSC Conference, XLVI: Abstract 2897.

Pierazzo, E., and H. J. Melosh (2000), Understanding oblique impacts from experiments, observations, and modeling, *Ann. Rev. Earth Planet. Sci.*, *28*, 141–167.

Pierazzo, E., A. M. Vickery, and H. J. Melosh (1997), A reevaluation of impact melt production, *Icarus*, *127*, 408–423.

Pilkington, M., and R. A. F. Grieve (1992), The geophysical signature of terrestrial impact craters, *Rev. Geophys.*, *30*, 161–181.

Potter, R. W. K., D. A. Kring, G. S. Collins, W. S. Kiefer, and P. J. McGovern (2013), Numerical modeling of the formation and structure of the Orientale impact basin, *J. Geophys. Res. Planets*, *118*, 963–979.

Reynolds, O. (1885), On the dilatancy of media composed of rigid particles in contact. With experimental illustrations, *Philos. Mag. J. Sci.*, *20*(S. 5), 469–481.

Soderblom, J. M., et al. (2015), The fractured Moon: Production and saturation of porosity in the lunar highlands from impact cratering, *Geophys. Res. Lett.*, *42*, 6939–6944, doi:10.1002/2015GL065022.

Thompson, S. L., and H. S. Lauson (1972), Improvements in the Chart D radiation-hydrodynamic CODE III: Revised analytic equation of state, (No. SC-RR--71-0714). Sandia National Laboratories, Albuquerque, N. M.

Wieczorek, M. A., et al. (2013), The crust of the Moon as seen by GRAIL, *Science*, *339*, 671–675.

Wünnemann, K., and B. A. Ivanov (2003), Numerical modelling of the impact crater depth–diameter dependence in an acoustically fluidized target, *Planet. Space Sci.*, *51*, 831–845.

Wünnemann, K., G. S. Collins, and H. J. Melosh (2006), A strain-based porosity model for use in hydrocode simulations of impacts and implications for transient crater growth in porous targets, *Icarus*, *180*, 514–527.

Yue, Z., B. C. Johnson, D. A. Minton, H. J. Melosh, K. Di, W. Hu, and Y. Liu (2013), Projectile remnants in central peaks of lunar impact craters, *Nat. Geosci.*, *6*, 435–437.

Zuber, M. T., et al. (2013), Gravity field of the Moon from the Gravity Recovery and Interior Laboratory (GRAIL) mission, *Science*, *339*, 668–671.